www.sciencemag.org/cgi/content/full/327/5970/1214/DC1

Supporting Online Material for

The Chicxulub Asteroid Impact and Mass Extinction at the Cretaceous-Paleogene Boundary

Peter Schulte,* Laia Alegret, Ignacio Arenillas, Jose A. Arz, Penny J. Barton, Paul R. Bown, Timothy J. Bralower, Gail L. Christeson, Philippe Claeys, Charles S. Cockell, Gareth S. Collins, Alexander Deutsch, Tamara J. Goldin, Kazuhisa Goto, José M. Grajales-Nishimura, Richard A. F. Grieve, Sean P. S. Gulick, Kirk R. Johnson, Wolfgang Kiessling, Christian Koeberl, David A. Kring, Kenneth G. MacLeod, Takafumi Matsui, Jay Melosh, Alessandro Montanari, Joanna V. Morgan, Clive R. Neal, Douglas J. Nichols, Richard D. Norris, Elisabetta Pierazzo, Greg Ravizza, Mario Rebolledo-Vieyra, Wolf Uwe Reimold, Eric Robin, Tobias Salge, Robert P. Speijer, Arthur R. Sweet, Jaime Urrutia-Fucugauchi, Vivi Vajda, Michael T. Whalen, Pi S. Willumsen

*To whom correspondence should be addressed. E-mail: schulte@geol.uni-erlangen.de

Published 5 March 2010, *Science* **327**, 1214 (2010)
DOI: 10.1126/science.1177265

This PDF file includes:

Materials and Methods

1. Mineralogy – The mineral composition of samples from the Ocean Drilling Project (ODP) Leg 207 Site 1259C and the Brazos River Cretaceous-Paleogene (K-Pg) sections was determined at the University of Erlangen on wet powdered samples (grain size <10 µm obtained with a McCrone Micromill) (*S1*) with a Siemens D5000 X-ray diffractometer. Powdered samples were scanned from 5° to 85° 2Θ with steps of 0.2° and a scanning time of 4 seconds. Spectra were evaluated by the quantitative Rietveld analysis with the BGMN Version 4.1.1 software (www.bgmn.de). The analytical error is <3% relative. Within BGMN, we used corrections for tube tails, sample zero point and sample eccentricity. The background was reduced to a 5-fold polynome to accommodate disordered phases. In addition, only the range between 10 and 65° 2Θ was fitted with BGMN to avoid problems in the high-angle range. The total number of parameters was 102-148, depending on automatic reducing the order of preferred orientation correction in cases of low phase content.

2. Stable isotopes – Samples from the K-Pg transition in the ODP Leg 207 Site 1259C were disintegrated in deionized water using a small amount of H_2O_2 then washed over a 63 µm sieve. Subsequently, the fine fraction (<63 µm) was separated and powdered. The fine fraction powder reacted with 100% phosphoric acid at 75°C using a Kiel III online carbonate preparation line connected to a ThermoFinnigan 252 mass spectrometer at the University of Erlangen (Germany). All values are reported in ‰ relative to VPDB by assigning a $\delta^{13}C$ value of +1.95 ‰ and a $\delta^{18}O$ value of –2.20 ‰ to NBS19. Reproducibility was determined by replicate analysis of laboratory standards and is better than ±0.05 and 0.06 ‰ (1σ) for $\delta^{13}C$ and $\delta^{18}O$, respectively.

3. Electron microprobe: Wavelength-dispersive (WDS) and energy-dispersive (EDS) electron microprobe (EMP) analyses, as well as back-scattered electron (BSE) images of ejecta components were performed with the JEOL JXA-8200 Superprobe (GeoZentrum Nordbayern, Universität Erlangen), equipped with four WDS spectrometers, an EDS system and an electron backscatter detector. In addition, at BRUKER AXS Microanalysis GmbH, Berlin, fast high-resolution element scans were conducted with a JEOL JSM-6490LV electron microscope equipped with a Quantax EDS system including a liquid nitrogen free XFlash 4010 and 4030 EDS silicon drift detector (SDD) and the Esprit 1.8 software using 15 kV acceleration voltage, counting rates between 100 and 220 kcps, and integration times of 10–20 min for a mapping resolution of 1600 x1200 pixel.

Supporting Text, Tables and Figures

Definition of the Cretaceous-Paleocene boundary

The base of the Danian Stage, i.e. Cretaceous-Paleogene (K-Pg; formerly K-T) boundary was formally delineated by the International Commission on Stratigraphy (ICS) at the base of the dark clay bed commonly called the “K-Pg boundary clay” in the Cretaceous-Paleogene Global Boundary Stratotype Section and Point (GSSP) at El Kef, Tunisia (*S2*). It is an undisturbed and continuos K-Pg boundary section and shows the coincidence of the mass extinction of marine plankton (calcareous nannofossils and planktonic foraminifera), ecological disruption at the sea floor (benthic foraminifera), drop in carbonate content, and perturbation of the global carbon cycle at the impact level [Fig. S1, (*S2*)]. This impact level, which we correlate to the Chicxulub impact, is present at base of the boundary clay and is characterized by a millimeter thick red clay layer that includes an Ir anomaly, ejecta spherules, and Ni-rich spinel (*S2*). There is no evidence for major extinctions or trends indicating ecological stress such as temperature change foreshadowing the K-Pg event in this section (*S3*-*S5*). Meanwhile, several auxiliary K-Pg boundary sections have been proposed and correlated to the El Kef section, including the Aïn Settera and Ellès sections (Tunisia), the Caravaca and Zumaya sections (Spain), the Bidart section (France), and the El Mulato and Bochil sections (Mexico) (*S6*).

Chicxulub impact ejecta at the K-Pg boundary

The petrography, composition, and age of ejecta material present in K-Pg boundary sites match the suite of target rocks within the Chicxulub crater. These target rocks include granitic to gneissic basement of Pan-African or older age, and Jurassic-Cretaceous carbonates, black shales, and evaporites (e.g., *S7*-*S9*).

(i) Shocked zircons from the ejecta deposits in Beloc, Haiti, and the K-Pg boundary event deposit in several sites in North America yield common U-Pb ages of 545±5 million years ago (Ma), in agreement with the Pan-African basement ages reported from crystalline clasts in breccias from the Chicxulub crater (Table S2) (*S10*).

(ii) Relict glass particles and vesicular ejecta spherules with a composition similar to Chicxulub melt rocks and unshocked feldspar and gneiss fragments that match the granitic to gneissic basement of Chicxulub are present in the event deposit at several intermediate distance and distal K-Pg boundary sites (Fig. S3) (*S11*-*S16*).

(iii) Accretionary calcite and dolomite clasts showing evidence of strong thermal metamorphism and fragments of shallow water limestone and dolomite are present in the event deposit at several proximal to intermediate distance K-Pg boundary sites, e.g., from all K-Pg sites in northeastern Mexico, from Brazos, Texas (*S17*), Ocean Drilling Program (ODP) Site 171, northwestern Atlantic (*S12*), ODP Leg 174AX, northwestern Atlantic (*S17*), ODP Site 207, tropical western North Atlantic (Fig. 3 and Figs. S3 to S5) (*S16*). The presence of textures indicative of shock-metamorphism and thermal alteration in these carbonate clasts suggest that they were ejected by the Chicxulub impact.

(iv) High concentrations of carbon cenospheres and soot in the red K-Pg boundary clay from several sites in North America, Denmark, and New Zealand are interpreted to derive from incomplete combustion of coal or petroleum droplets, probably from Jurassic-Cretaceous black shales in the Yucatán carbonate platform close to Chicxulub (*S18*, *S19*).

(v) Kuiper et al. (*S20*) used a combination of orbital chronology and geochronology to arrive at a new estimate for the absolute age of the K-Pg boundary of ~65.95 million years ago. These authors provided also an assessment of geochronologic data constraining the ages of the Chicxulub impact crater and spherules from proximal to intermediate K-Pg boundary sections (see Table 1 in *S20*). Kuiper et al. (*S20*) concluded that there is no indication that the age of the Chicxulub impact melt lithologies predate the K-Pg boundary by 300 thousand years and indicated that rather the available ages of Chicxulub melt rocks and the shocked minerals and ejecta spherules from the K-Pg boundary in Northern America are indistinguishable within an uncertainty of <100 thousand years.

(vi) Alvarez et al. (*S21*) report a one million year-long iridium record from Gubbio, Italy, demonstrating that this well documented pelagic sequence contains no evidence of multiple Ir anomalies. This result was recently confirmed by additional high resolution iridium data from a nearby section and two additional ocean drilling sites complemented by associated Os isotope data (*S22*) (see also Fig. S16 for a partial reproduction of the Os isotope data).

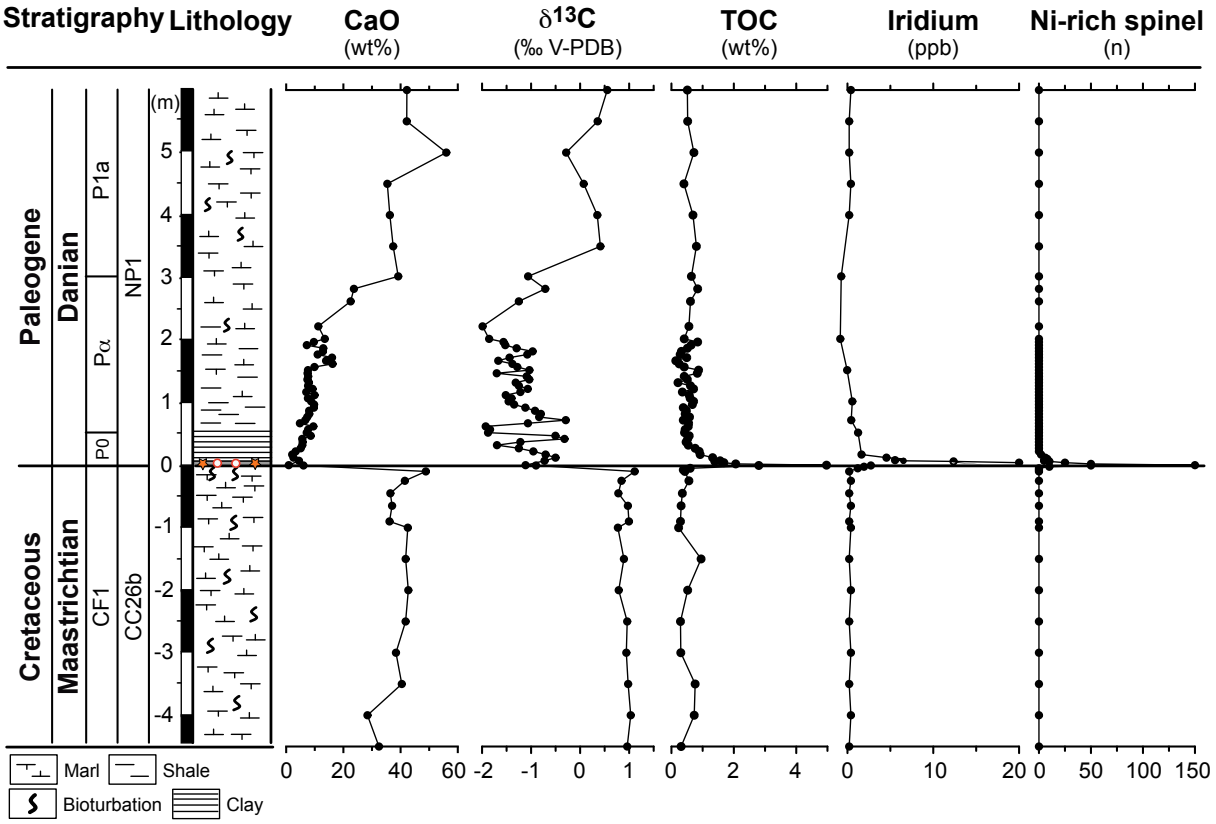

Figure S1. Integrated stratigraphy and geochemistry across the K-Pg boundary in the El Kef GSSP section ($\delta^{13}C$ data derived from bulk rock analysis; data compiled from *S2*, *S5*, *S23*, S*24*).

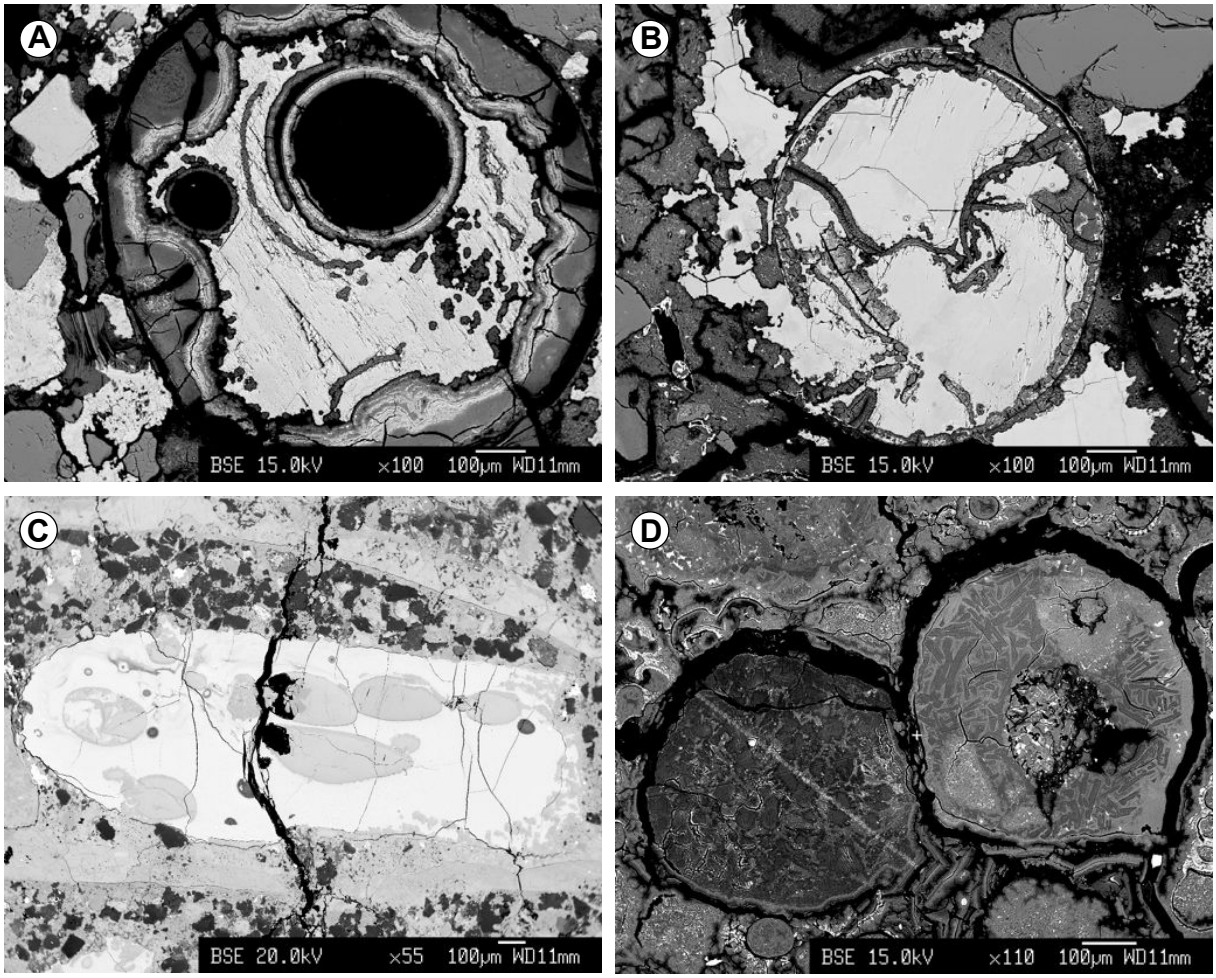

Figure S2: Backscattered-electron (BSE) images of typical ejecta spherules from the K-Pg event deposit. (**A**) and (**B**) Rounded and vesicular spherules from the Shell Creek site, Alabama (see *S25* for locality and lithology) that consist of a smectite shell and a calcite infilling. Note welding of two spherules in (B). (**C**) A dumbell-shaped spherule from the La Popa Basin, Mexico (sample from the base of section E4 in *S26*). The bright gray appearance of the spherule results from the high Fe- and Mg-contents that is a typical feature of the spherules in northeastern Mexico (*S27*). (**C**) Two smectite spherules from the ODP Leg 207, Demerara Rise, western tropical North Atlantic. Difference in grey tones result from different smectite compositions with the spherule to the right showing significant higher Fe- and Mg-contents than the spherule to the left. Note also presence of smectite pseudomorphs after lath-shaped crystals which represent a primary feature that reflects rapid cooling from a melt (*S16*).

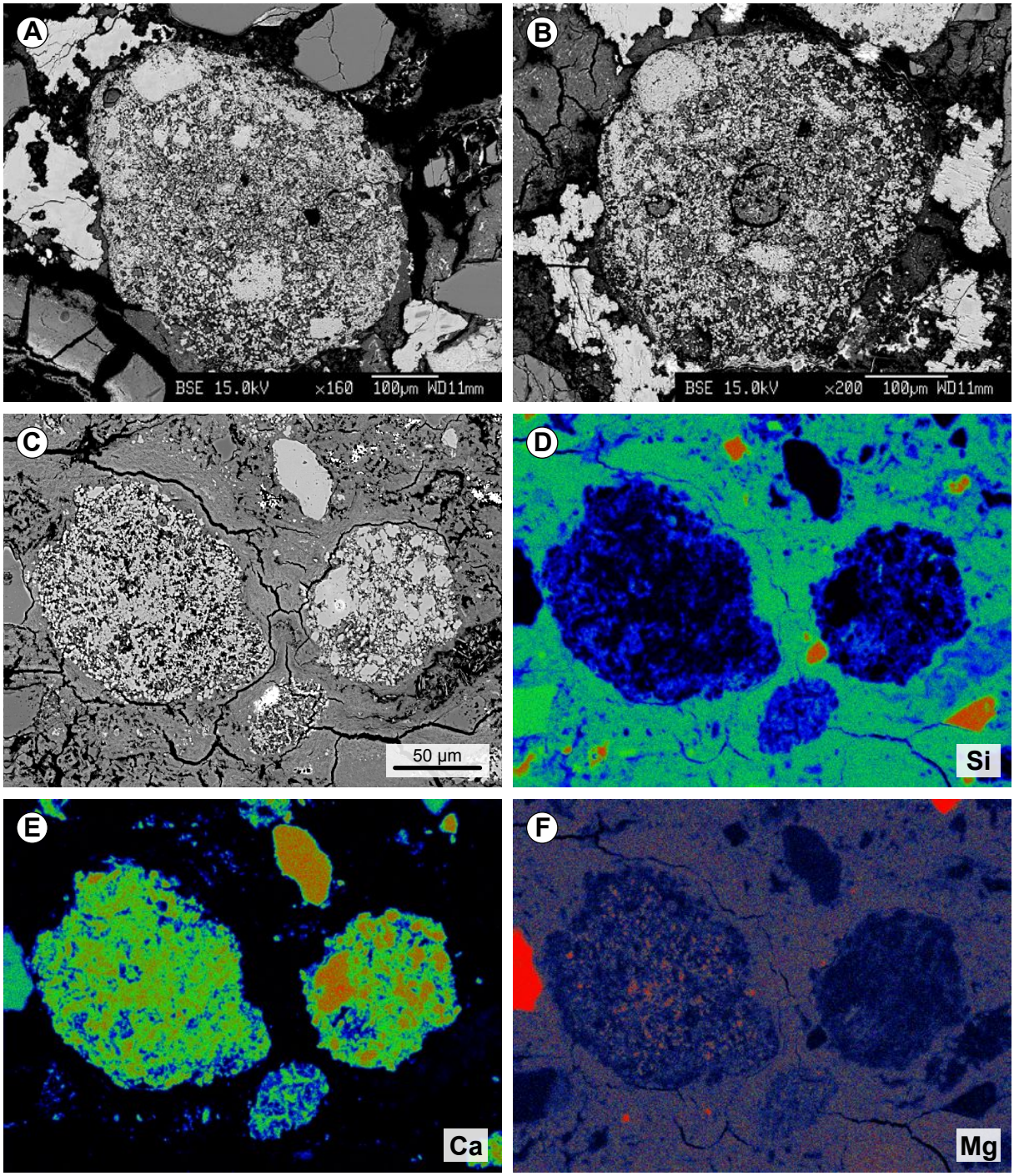

Figure S3: Accretionary carbonate clasts from the K-Pg event deposit. (**A**) and (**B**) BSE images of typical carbonate clasts from the Shell Creek site, Alabama which are similar to the carbonate clasts described from the Brazos site, Texas (*S17*). (**C**) to (**F**) BSE image and energy-dispersive (EDS) elemental maps from two accretionary carbonate clasts from the topmost 0.5 mm of the event deposit in ODP Leg 207, Demerara Rise, West Atlantic (see also Fig. 3). Note slight enrichment of Mg in the left clast. Spectrum from black to blue, green, and red corresponds to increasing element abundance.

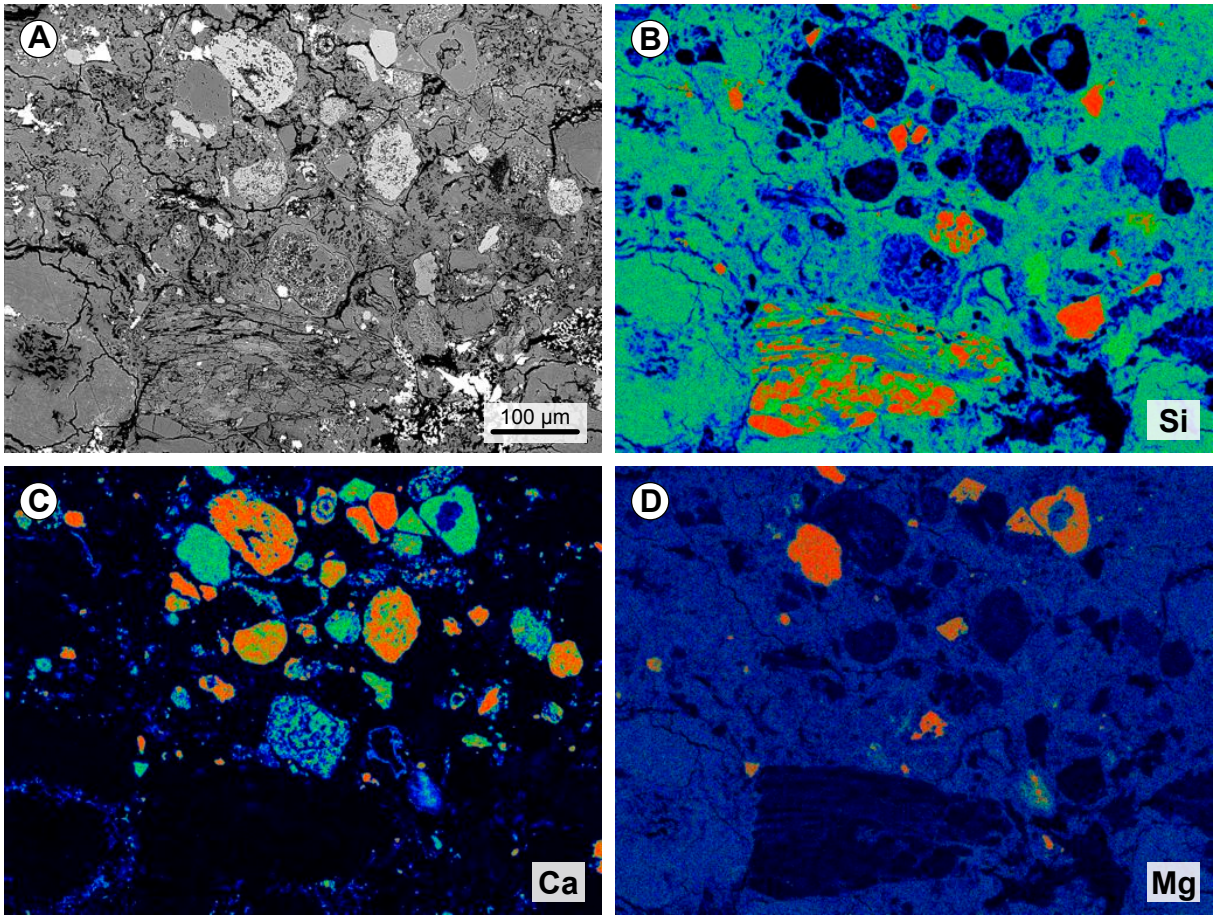

Figure S4: BSE image and EDS elemental maps showing the topmost 0.5 mm of the event deposit in ODP Leg 207, Demerara Rise, tropical western North Atlantic. Note complex composition of the event bed with various types of accretionary carbonate clasts, dolomite clasts, large lithic, quartz grains, and a large lithic clast in the lower part consisting of feldspar, mica, and quartz. This grain is 200 x 350 µm in size and probably a gneiss clast (*S16*). For additional details see Fig. 3.

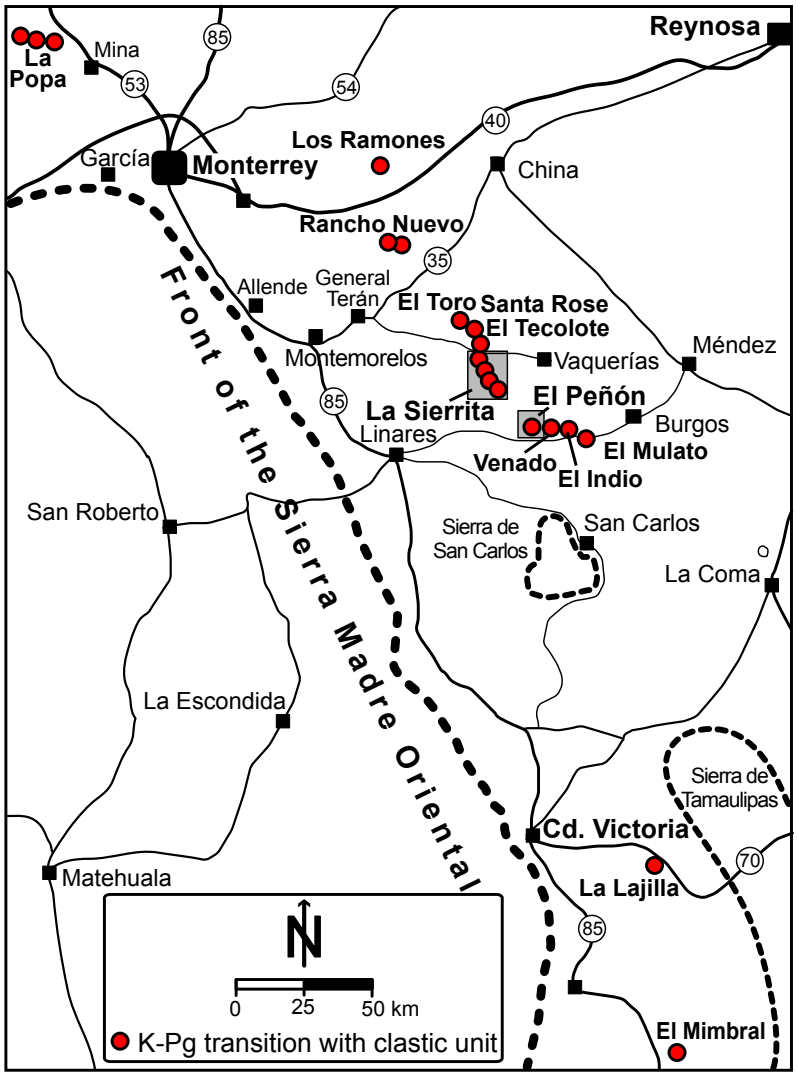

Figure S5: Overview map of the K-Pg boundary sections in NE Mexico. Note that slumped, lens-like ejecta deposits within upper Maastrichtian marls have only been reported from two outcrops (La Sierrita and El Peñón) (*S28, S29*).

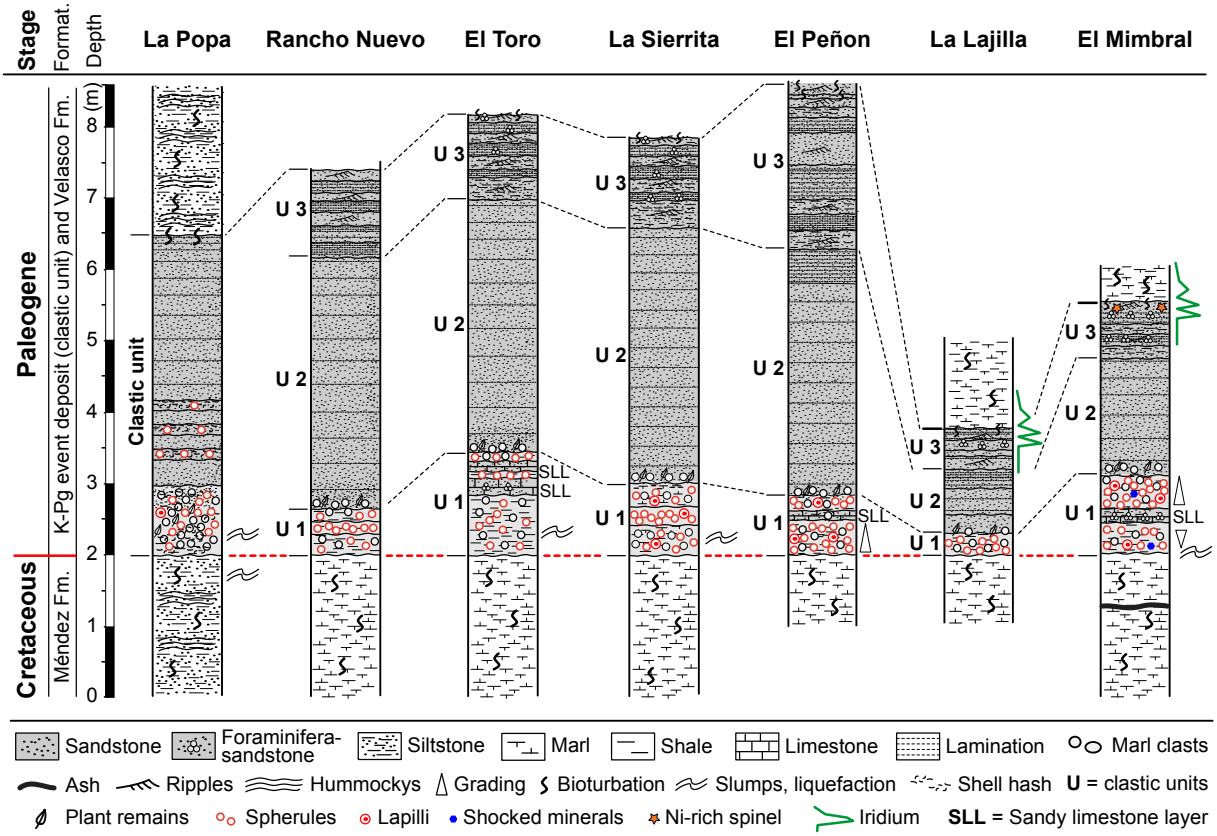

Figure S6: Schematic lithological columns of the clastic unit in NE Mexico. This transect spans the northernmost K-Pg boundary sections outcrops in the La Popa Basin up to the El Mimbral outcrop. Note similarity of the depositional sequence across a distance of 300 km (compiled from *S26*, *S27,* and *S30*). The sedimentary sequence in the La Popa basin is distinct as this is a inner neritic setting, compared to the bathyal settings of all other K-Pg sites in NE Mexico. Ir abundance schematically drawn after Smit et al. (*S30*) for the El Mimbral sections, and after Lindenmaier et al. (*S31*) for the La Lajilla sections. Ni-rich spinel data are from Rocchia et al. (*S24*).

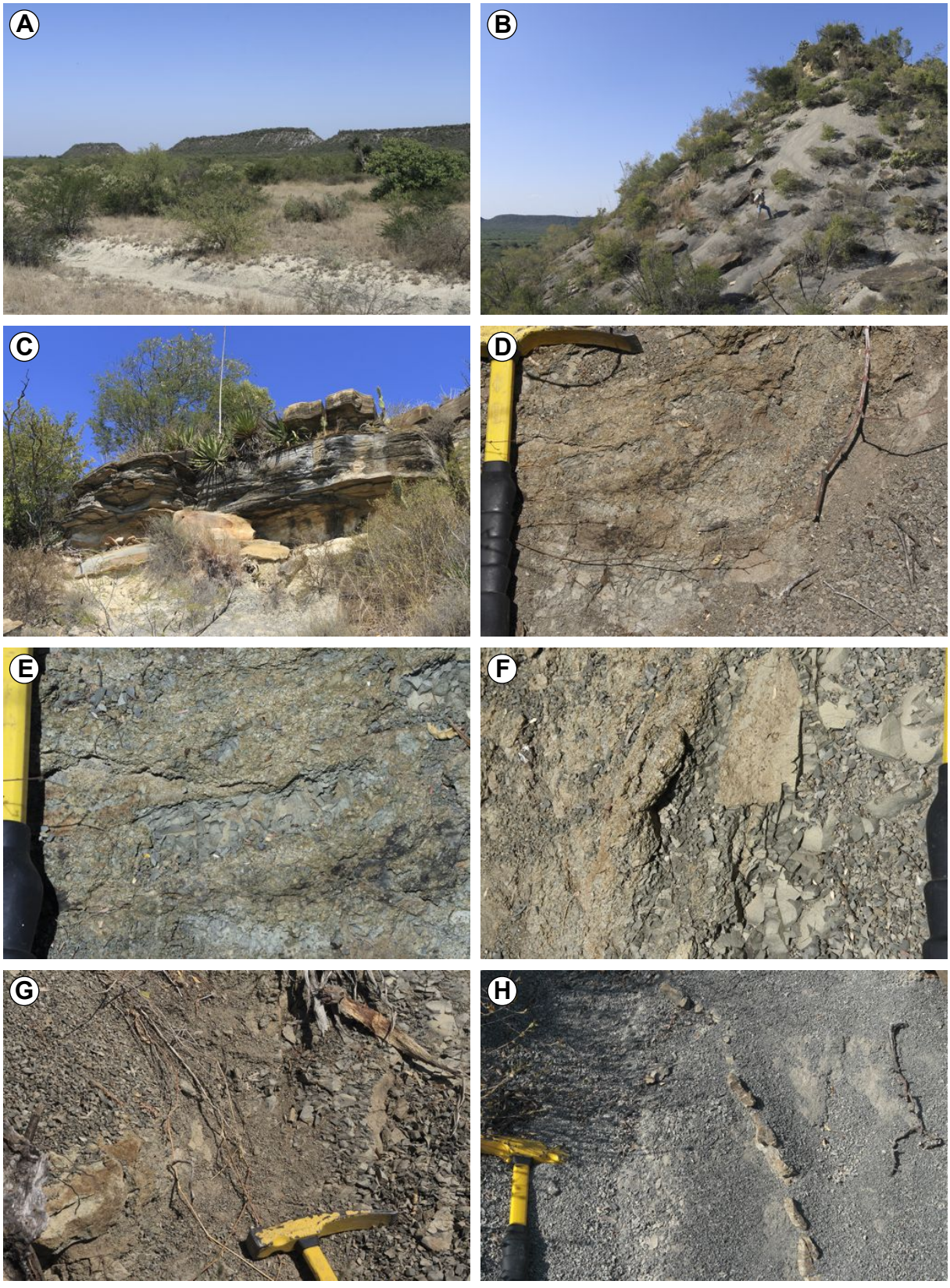

Figure S7: (caption on next page)

Figure S7 (page 11): Outcrop photos of the clastic unit and the disturbed Chicxulub ejecta deposit in the La Sierrita area (for additional details see *S28, S29*). (**A**) Succession of hills showing from right to left the Loma and the two Loma Cerca hills with the K-Pg clastic unit on top. (**B**) View on the Northern Loma Cerca showing the excellent exposures of the upper Maastrichtian marls along the flanks of the hills. No evidence for multiple laterally continuos “layers” of ejecta spherules is present. (**C**) Clastic deposit on top of the Loma Cerca. (**D** to **G**) Large “blobs” of slump folds and marl-spherule mixtures that are irregularly exposed for a few centimeters to several meters along the south-western flank of the Loma Cerca indicating pervasive soft-sediment deformation. (**H**) Thin red siltstone layers that are intercalated within the upper Maastrichtian marls below the spherule deposit. Their strike and dip (125°/40°) is clearly different from the nearly horizontally-lying clastic unit and indicates remobilization of upper Maastrichtian Méndez marls before deposition of the clastic unit. Hammer for scale (30 cm), top of hammer shows upsection.

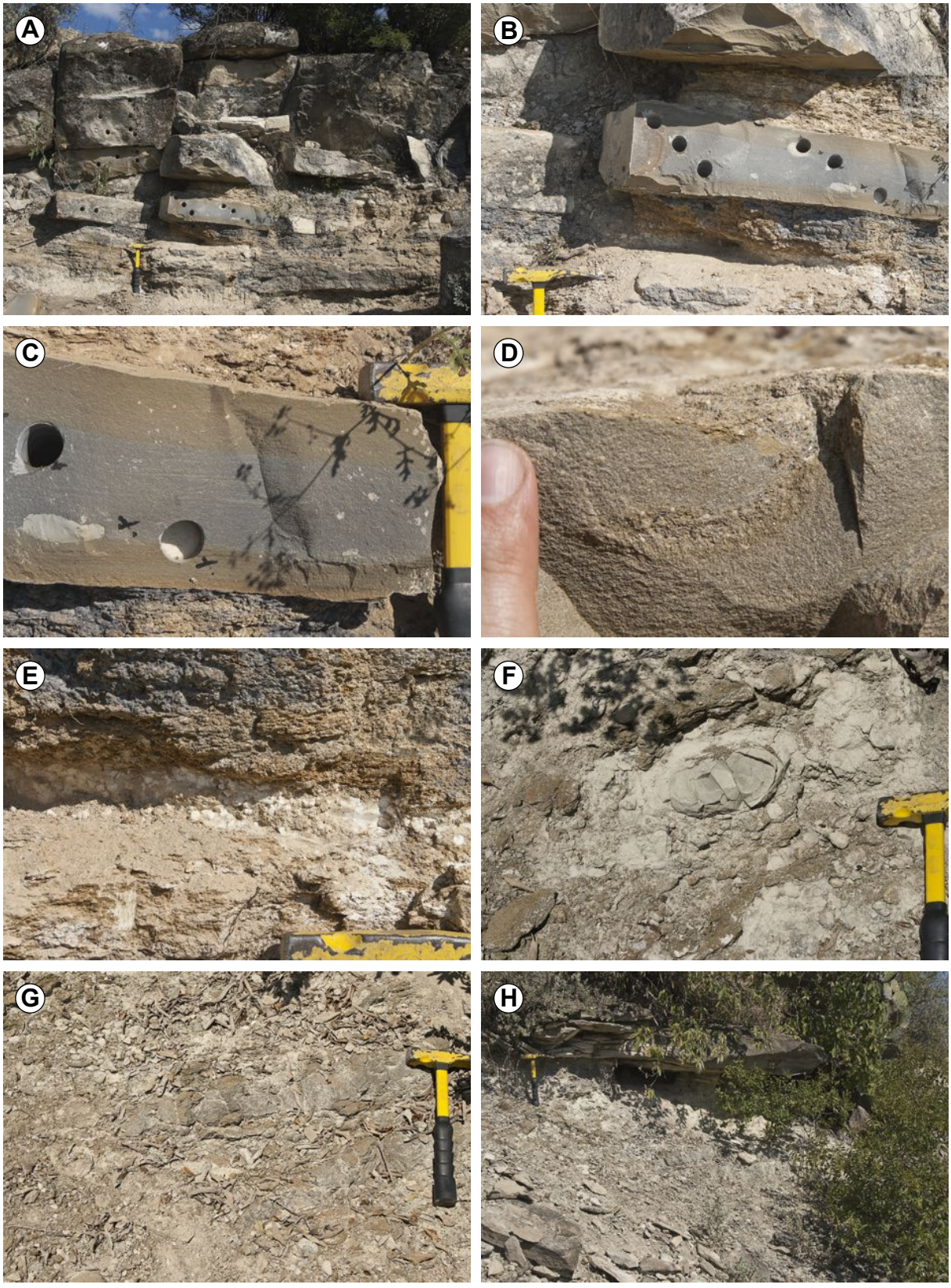

Figure S8 (caption on next page).

Figure S8 (page 13): Outcrop photos of the clastic unit and the disturbed ejecta deposit in the El Peñón area. (**A**) Clastic deposit in the main quarry section. Note different dip directions of the lower part compared to the upper part of the section; hammer marks the base of the clastic deposit. (**B**) Detail of the basal part of the clastic deposit showing the spherule layer intercalated by a 10 cm-thick calcareous sandstone layer. (**C**) Detail of the calcareous sandstone showing large rip-up clasts at the base and faint lamination in the upper part. (**D**) The famous single J-shaped structure in the calcareous sandstone layer that was interpreted by Keller et al. (*S32*) as a burrow and as evidence for long-term deposition. However, besides this single structure at El Peñón, no evidence for bioturbation was observed in the up to 10 m thick, massive sands of the clastic unit in the outcrops of the La Popa, Rancho Nuevo, La Sierrita, El Mulato, La Lajilla, El Mimbral, or La Ceiba area (Figs. S6 to S8) (*S27*, *S30*, *S33*). Obviously, the presence of tracemakers is an extremely rare phenomenon in the northeastern Mexican clastic unit and confined to the top of the clastic unit. (**E**) Base of the spherule deposit with intercalated 3-cm thick layer of accretionary calcite spherules. (**F** and **G**) Slumped spherule deposit with large marl clasts about 200 m to the southeast of the main quarry outcrop showing doubling of spherule layer and mixing with upper Maastrichtian marls. (**H**) About 400 m from the main quarry outcrop to the southeast, the spherule deposit is again overlain by sandstone from the clastic unit (additional details in *S27*).

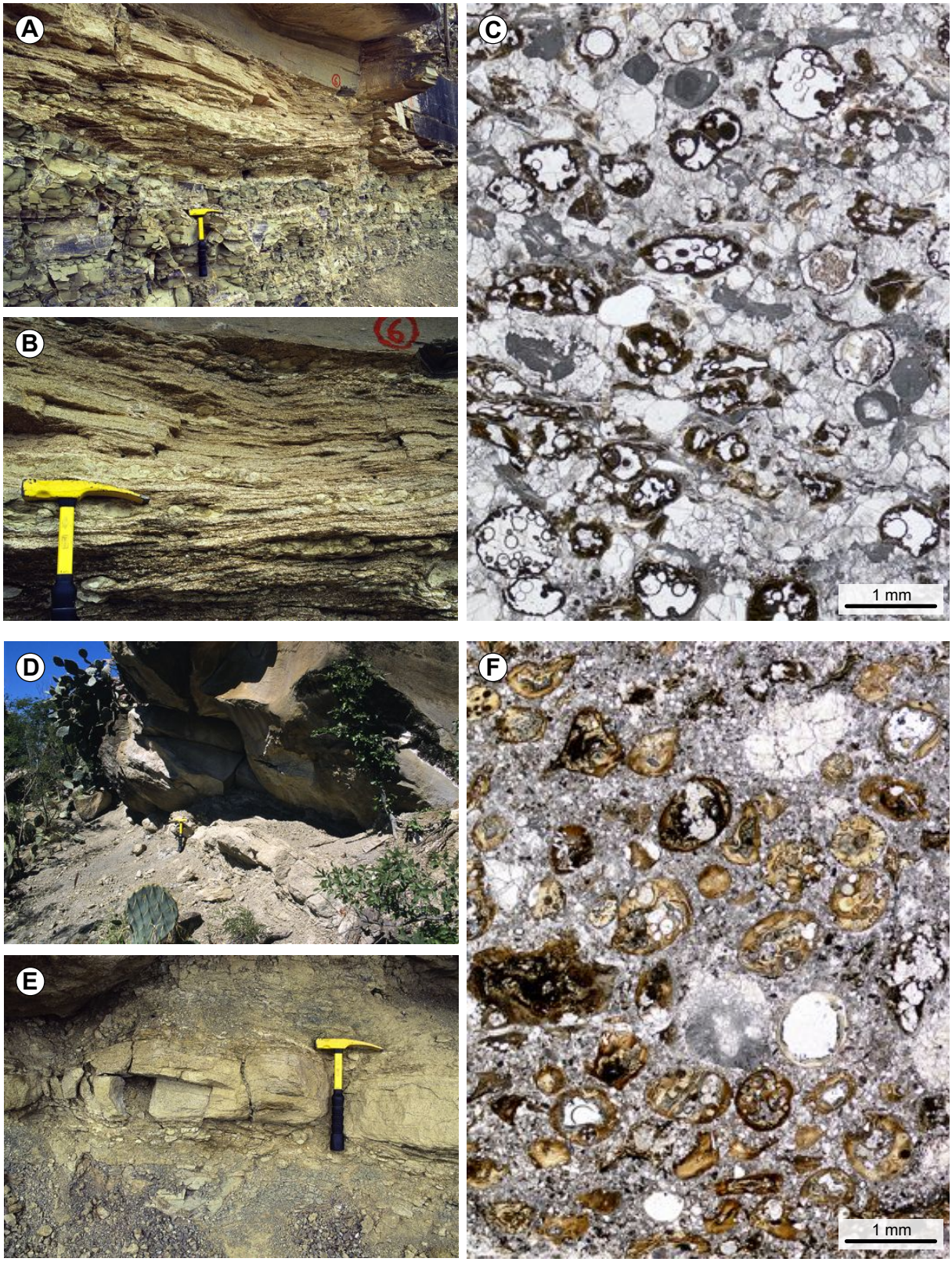

Figure S9 (caption on next page).

Figure S9 (page 15): Outcrop and corresponding thin-section photos of the basal ejecta bed of the clastic unit in northeastern Mexico. (**A**) Spherule deposit at El Mimbral at meter-mark 6. Note through-like wavy upper surface of the Méndez marls and presence of thin bentonite layer (at top of the hammer) below the laminated spherule bed similar to yellow clay layer the Cottonmouth Creek, Brazos (see Fig. S11). (**B**) Graded and laminated spherule deposit at El Mimbral. Note coarse, cm-sized ejecta (spherules and carbonate clasts), as well as marl clasts at the base. (**C**) Photomicrograph showing abundant spherules, limestone clasts, and blocky carbonate. (**D)** Spherule deposit at the Mesa Juan Perez 1A section showing alternating layers of weathered marl and spherule layers under- and overlying the indurated calcareous spherule layer. (**F**) Close-up of the laminated spherule layers showing alternating white layers of carbonaceous and spherule-rich ejecta. (**G**) Photomicrograph showing ejecta spherules, carbonate clasts, and minor fine-grained terrigeneous debris (e.g., quartz, feldspar). The presence of delicate petrographical structures, the compositional complexity of the deposit, and the absence of abrasion features or sorting suggests that this is a primary deposit with only minor transport at the seafloor.

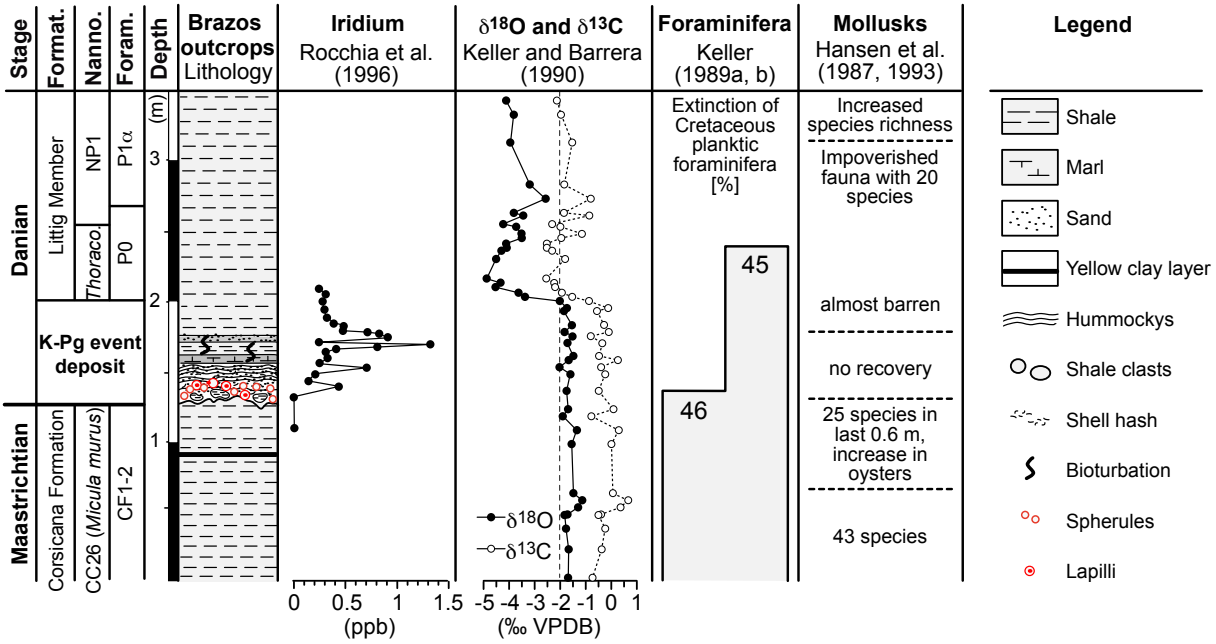

Figure S10: The K-Pg boundary in the Cottonmouth Creek, Brazos. A similar iridium distribution has been reported by Hansen et al. (*S34*) and Heyman et al. (*S35*).

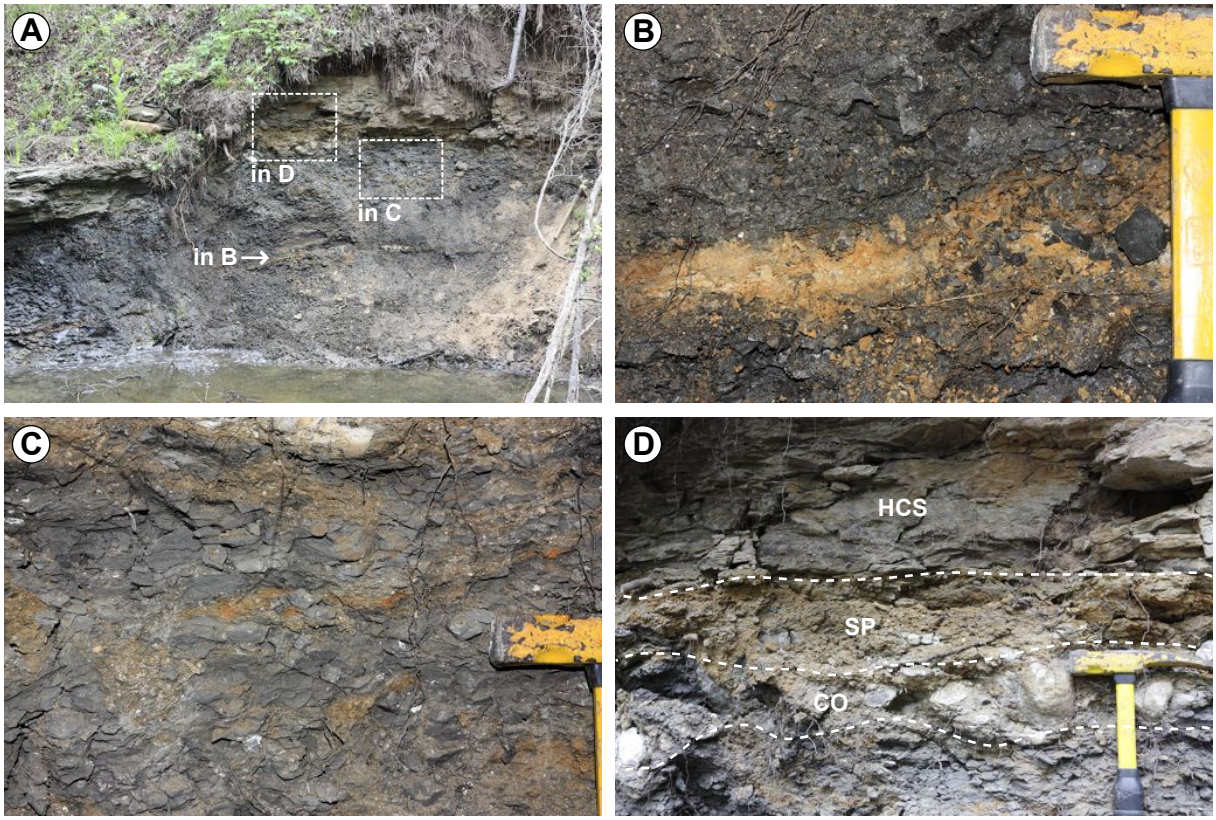

Figure S11: The K-Pg boundary at Brazos, Texas. (**A**) Overview of the K-Pg boundary interval at the Cottonmouth Creek, Brazos. (**B**) The upper Maastrichtian yellow clay layer was considered by Keller et al. (*S36*) as original Chicxulub ejecta. Our petrographical and mineralogical analysis – showing high quartz and sanidine contents – clearly contrasts with data for the Chicxulub ejecta layer (Table S3 and Fig. S12) and strongly indicate a volcanic origin of this yellow clay layer. Similar thin ash layers have been observed in upper Maastrichtian sections in northeastern Mexico and Haiti (Fig. S9) (*S37*, *S38*). (**C**) Disturbed uppermost Maastrichtian shales with large shale clasts separated by reddish, shell-rich clasts. (**D**) The K-Pg boundary event deposit consisting of a normally-graded, basal conglomeratic layer ("CO") with ejecta spherules, concretions, and shell hash, overlain by the spherule deposit ("SP") followed sequentially upward by repeated upward fining units of hummocky cross-bedded and laminated silicic and calcareous sands ("HCS"), which are burrowed in their uppermost parts, and then by a upward-fining silty shale unit (Fig. S7) (*S34*, *S35*, S39-*S41*). The K-Pg boundary is placed at the base of the ejecta-rich clastic unit (e.g., *S30*, *S41*-*S43*).

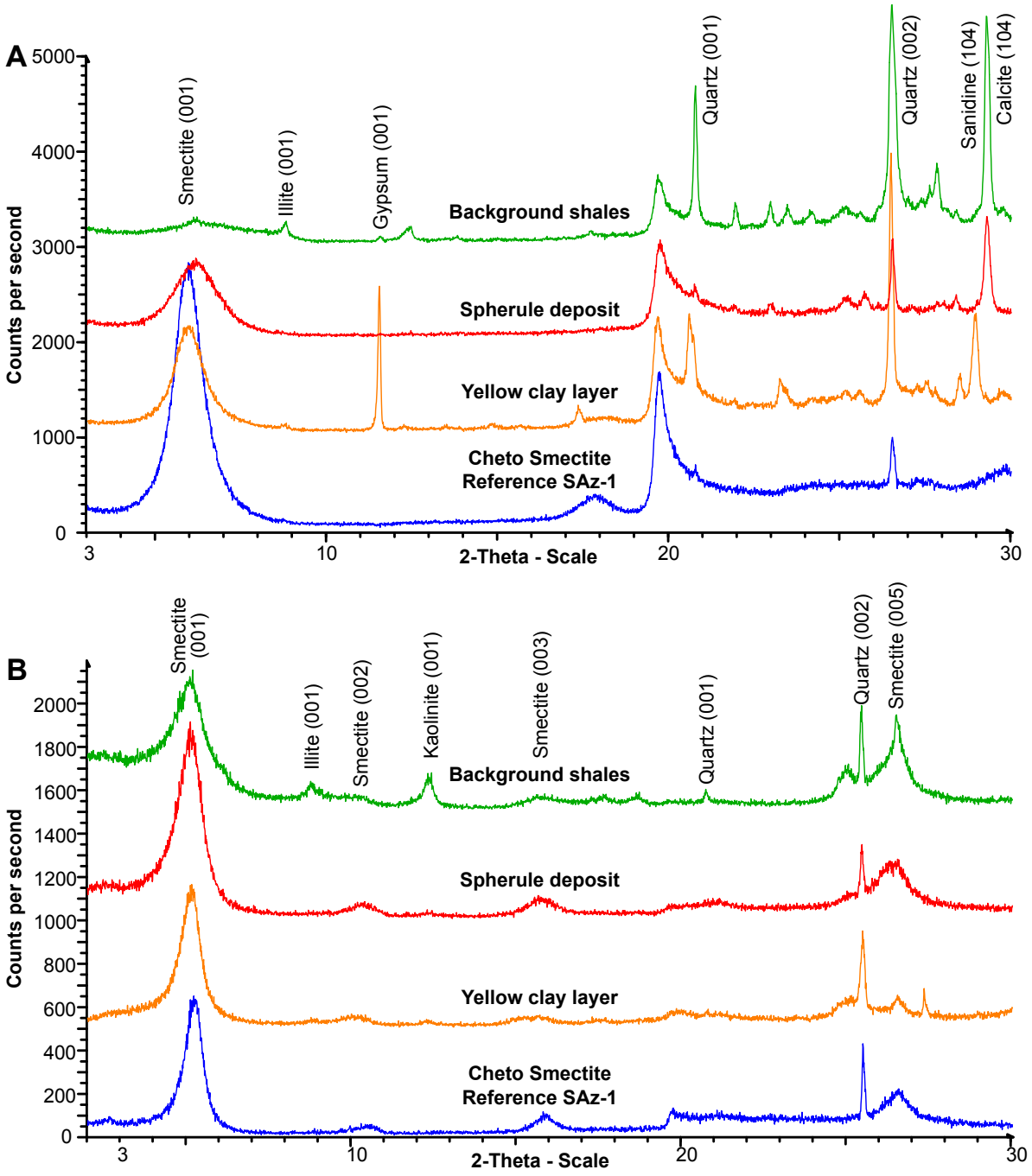

Figure S12: Mineralogy of the Brazos K-Pg section. (**A**) Bulk rock mineralogy and (**B**) clay mineralogy of the K-Pg boundary ejecta bed, the upper Maastrichtian yellow clay layer, and the background shales from the Cottonmouth Creek K-Pg section, Brazos, compared to the Cheto smectite from Arizona as reference (source clay SAz-2 as provided by the Clay Minerals Society, *S44*). Note differences in XRD patterns and specifically the high sanidine content of the yellow clay layer and absence of calcite, strongly suggesting a volcanic origin.

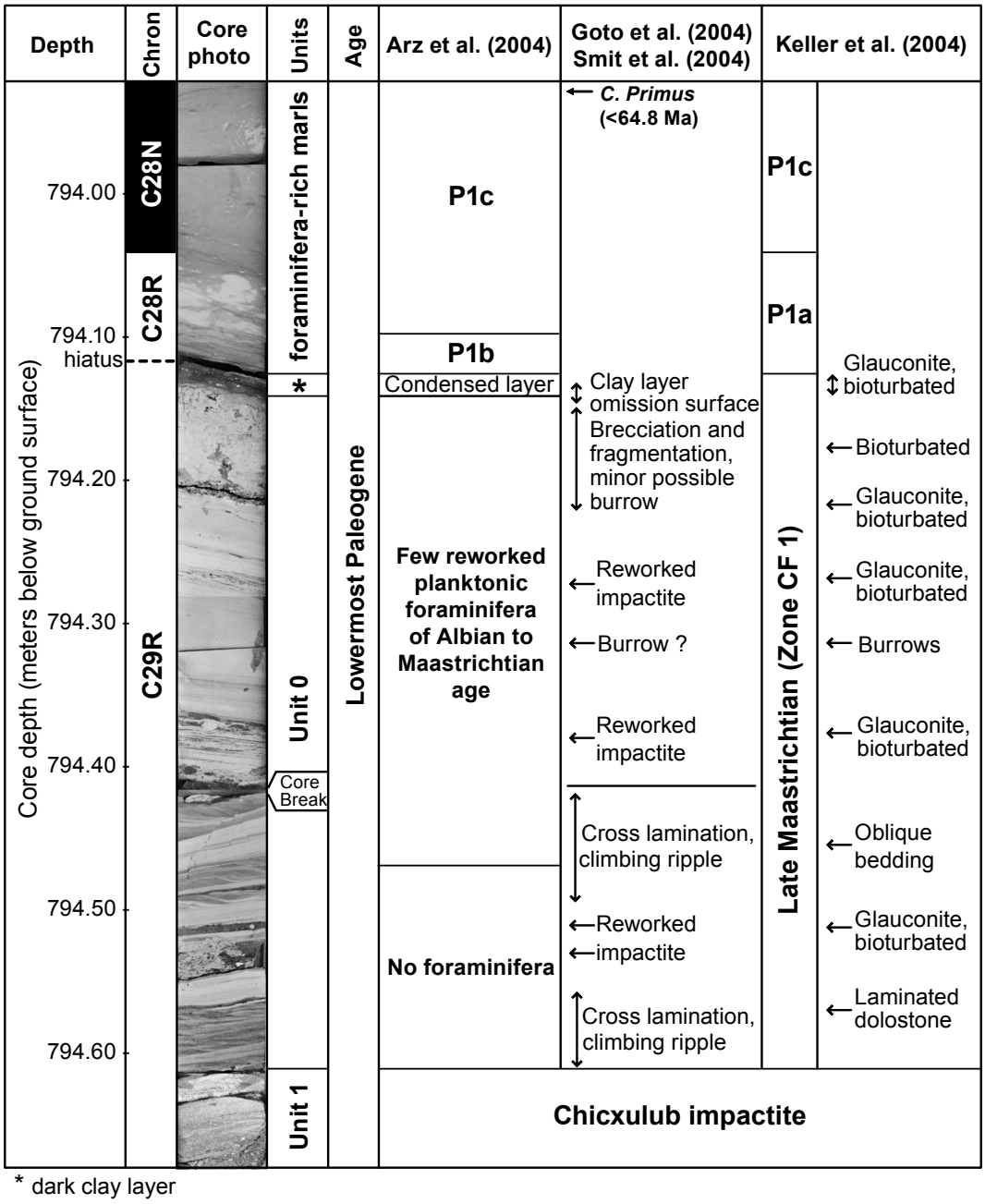

Figure S13: K-Pg boundary in core Yaxcopoil-1 – Photograph of the transition from the Chicxulub impact breccia to the lower Paleocene (modified after *S45*) showing observations from Goto et al. (*S46*), Arz et al., (*S47*), and Smit et al. (*S48*) versus Keller et al. (*S49*). The magnetostratigraphy is from Rebolledo-Vieyra and Urrutia-Fucugauchi (*S50*). Note that a distinct K-Pg boundary red clay layer (i.e., with an Ir anomaly, shocked minerals etc.) is lacking. Arz et al. (*S47*), Goto et al. (*S46*), and Smit et al. (*S48*) located the K-Pg boundary at the base of the impact sequence (at 894,94 m in core depth), according to the original definition of this boundary in the El Kef section, Tunisia (*S2*).

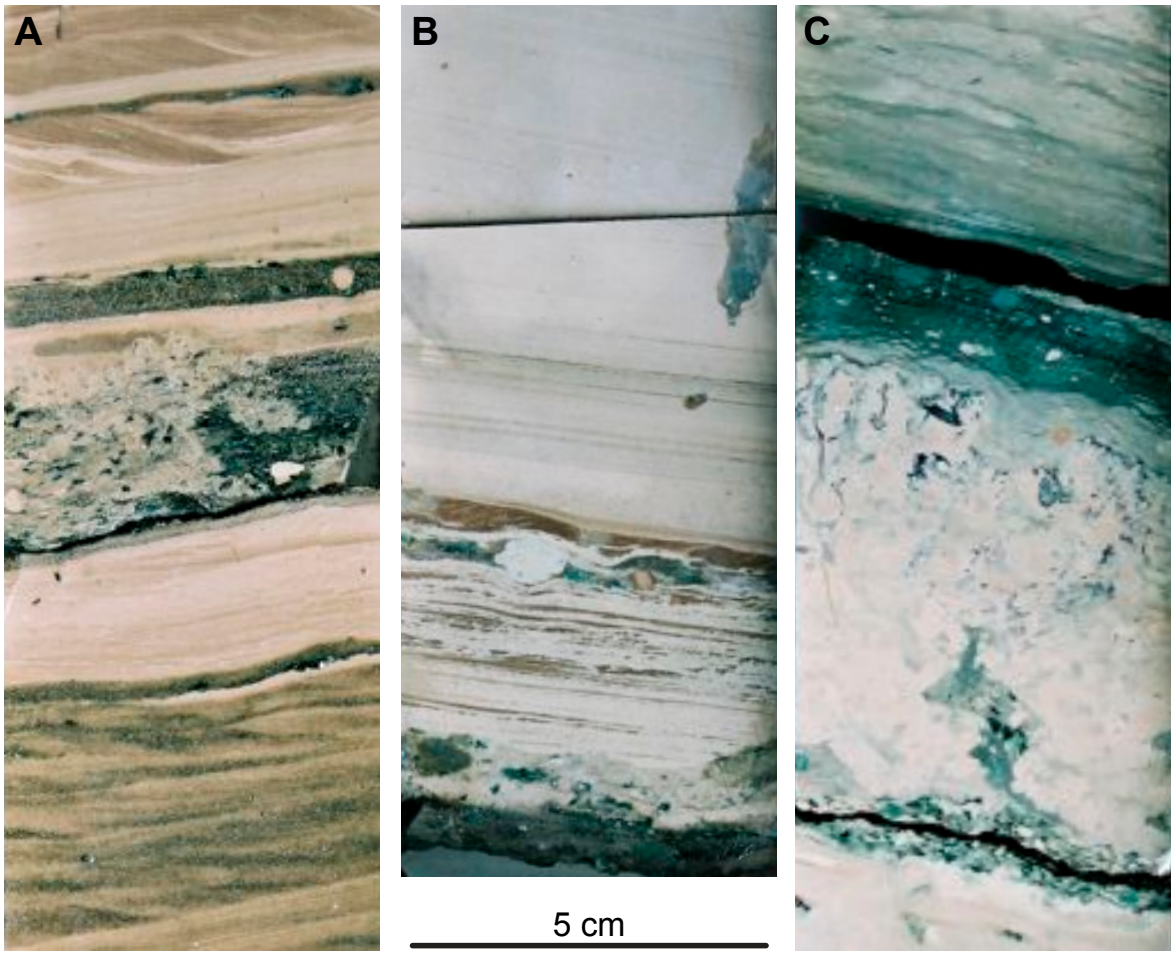

Figure S14: K-Pg boundary in core Yaxcopoil-1 – Close up photographs from (**A**) the lower part of unit 0 showing climbing ripples and cm-thick layers of ejecta-rich material, (**B**) the middle part of unit 0 with lamination and intercalated layers of ejecta-rich material; note that there is no bioturbation in the greenish sandstone layer, only the tube-like structure to the upper right may be a burrow (**C**) the condensed clay layer that overlies the uppermost part of unit 0 with an irregular erosion surface (modified after *S45*).

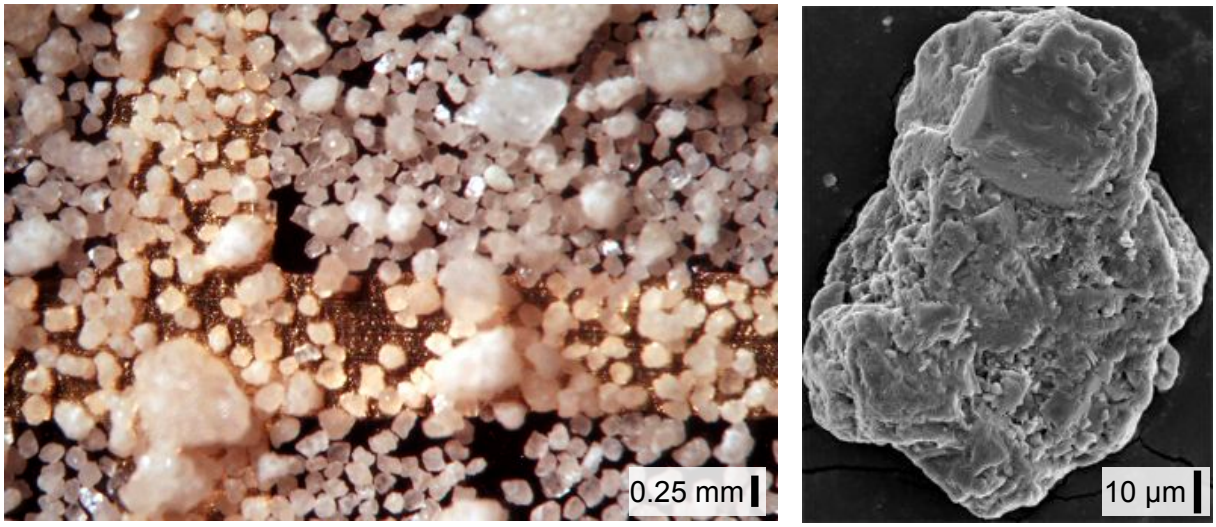

Figure S15: K-Pg boundary in core Yaxcopoil-1 – (**A**) Photographs of the washed residue showing abundant dolomite crystals as well as amalgamated dolomite crystals in a sample from the 794.55 m in core depth. This sample is equivalent to the sample Yax-20 of Keller et al. (*S49*) in which they allegedly identified the greatest planktonic foraminiferal diversity. (**B**) Scanning electron microscope image of an amalgamated dolomite clast that superficially resembles a planktonic foraminifer (at 794.55 m in core depth).

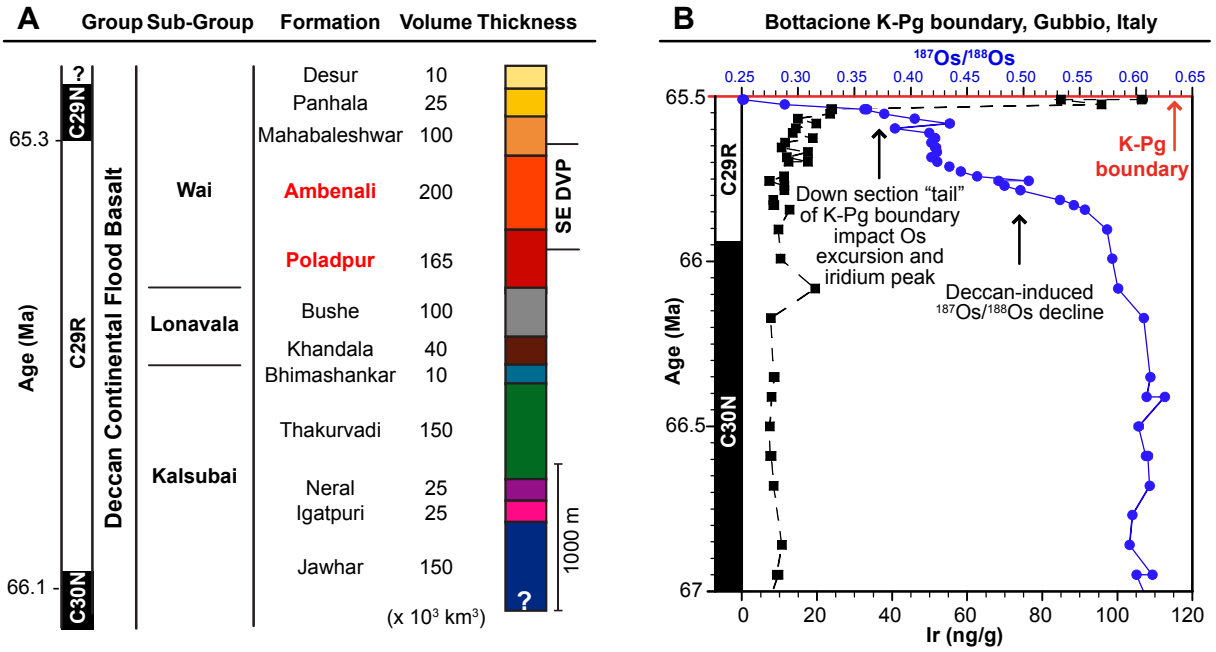

Figure S16: Compilation of the stratigraphic data for the emplacement phases of the Deccan flood basalts in southwest India. (**A**) Overview on stratigraphy, thickness, and volume of the lava flows (e.g., *S51*). Because the C29r/C29n reversal occurs in the lower Mahabaleshwar, the K-Pg boundary is most likely likely within the Poladpur and Ambenali formations marked in red, although the exact stratigraphic position has not been determined. (**B**) Os isotope data that are interpreted to show the onset of massive Deccan volcanism during the lower part of magnetochron C29r (*S22*).

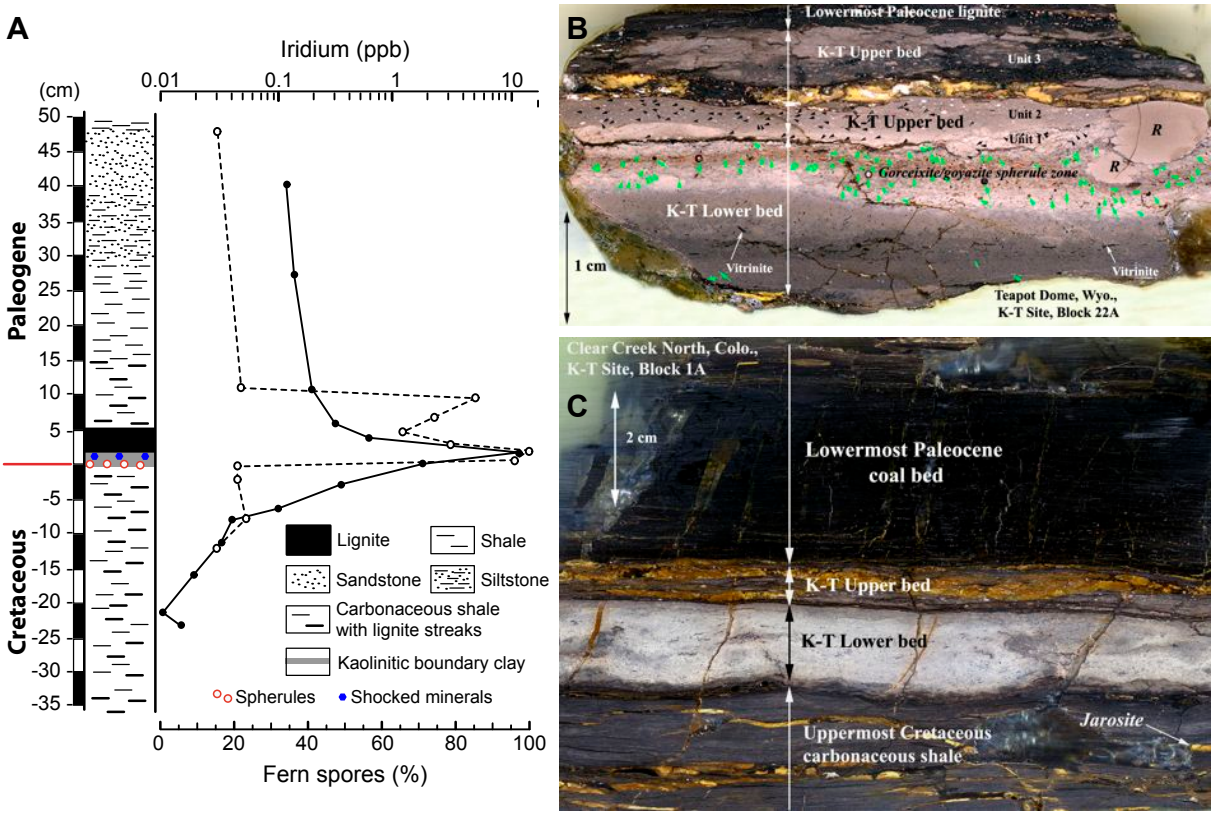

Figure S17: The K-Pg boundary in the Western Interior. (**A**) Schematic lithology of the K-Pg boundary interval at the Starkville North site, 5 km south of Trinidad, Colorado. The large black dots and the solid line show the iridium concentration, the open circles and the dashed line show the fern spore percentages (modified after *S52*). (**B**) Polished surface of the dual-layer K-Pg boundary claystone at the Teapot Dome site, Wyoming. Green arrows show ejecta spherules that are now altered to alumino-phosphate (gorceixite, goyzite) in the lower claystone. Black arrows show detrital quartz (shocked and unshocked) that is abundant in the upper claystone. Two large rip-up claystone clasts are marked with "R". Photo courtesy of Glen A. Izett. (**C**) Polished surface of the K-Pg boundary interval at the Clear Creek North site, Colorado. The lower K-Pg claystone bed consists of kaolinite clay and minor amounts of illite-smectite (I-S) mixed-layer phyllosilicates. Typically, this bed contains shreds and deformed laminae of vitrinite. This bed also contains ejecta spherules altered to kaolinite and alumino-phosphate. The upper part of the K-Pg claystone couplet is again compositionally and texturally different from the lower bed. It consists predominantly of illite-smectite (I-S) mixed-layer phyllosilicates and minor kaolinite and contains an assemblage of detrital silicate mineral grains (shocked and unshocked). Highest concentrations of the platinum group elements (PGEs) are usually present in the upper layer. Photo courtesy of Glen A. Izett.

Table S1: Key locations that show a detailed and expanded record across the K-Pg boundary including evidence for the presence of impact ejecta. See Fig. 1 for location of DSDP and ODP sites; color code for comparison with Fig. 2.

Region and K-Pg boundary sites	Distance*	Impact ejecta**	Max. Iridium concentration	Setting***	References
	(km)		(ppb)		
Very proximal to Chicxulub: 10 to >80 m-thick K-Pg boundary event deposit					
Southern Mexico and Cuba					
Guayal, Tabasco	300	SP, SQ, NI	0.8	Bathyal	(*S53-S55*)
Bochil, Chiapas	300	SP, SQ, NI	1.5	Bathyal	(*S6*, *S53-S55*)
Albion Island, Belize	300	SP, SQ	n.a.	Terrestrial	(*S56-S58*)
Moncada, Cuba	400	SP, SQ	0.5	Bathyal	(*S59*)
Loma Capiro, Santa Isabel, Peñalver, Cacarajícara, and Cidra, Cuba	400	SP, SQ	n.a.	Bathyal	(*S59-S62*)
Proximal to Chicxulub: dm to 10 m-thick K-Pg boundary event deposit					
Gulf of Mexico					
Beloc, Haiti	500	SP, SQ, NI	28	Bathyal	(*S63-S65*)
La Ceiba, Mexico	700	SP, SQ, NI	n.a.	Lower bathyal	(*S30*, *S33*, *S66*)
El Mimbral, Mexico	700	SP, SQ, NI	0.5	Lower bathyal	(*S27*, *S30*, *S66*)
La Lajilla, Mexico	750	SP, AC	0.25	Lower bathyal	(*S30*, *S66*)
El Mulato, Mexico	780	SP, AC	1	Lower bathyal	(*S6*, *S30*)
El Peñón, Mexico	800	SP, AC	n.a.	Middle bathyal	(*S27*, *S30*, *S66*)
La Sierrita, Mexico	800	SP, AC	0.3	Middle bathyal	(*S27*, *S28*, *S66*)
La Popa Basin, Mexico	800	SP, AC	n.a.	Inner neritic	(*S26*, *S67*)
Brazos River, Texas	900	SP, AC	n.a.	Neritic	(*S17*, *S30*, *S41*, *S43*)
Stoddard County, Missouri	900	SP	n.a.	Neritic	(*S68*)
Mussel Creek, Shell Creek, Antioch Church Core, Millers Ferry, Alabama	900	SP, AC	n.a.	Neritic	(*S25*, *S30*, *S69*)
Caribbean Sea					
ODP Leg 165: Site 999 and 1001	600	SP	n.a.	Bathyal	(*S70*)
Intermediate to Chicxulub: 1 to 10 cm-thick K-Pg boundary event deposit					
Western Interior (USA and Canada)					
Sugarite, Raton Basin, New Mexico	2100	SP, SQ (FS)	2.7	Terrestrial	(*S71-S73*)
Starkville South, Raton Basin, Colorado	2250	SP, SQ (FS)	56	Terrestrial	(*S71-S73*)
Starkville North, Raton Basin, Colorado	2250	SP, SQ (FS)	6	Terrestrial	(*S71-S73*)

Region and K-Pg boundary sites	Distance*	Impact ejecta**	Max. Iridium concentration	Setting***	References
	(km)		(ppb)		
Long Canyon, Raton Basin, Colorado	2250	SQ (FS)	8.2	Terrestrial	(*S73*, *S74*)
Berwind Canyon, Raton Basin, Colorado	2250	SP, SQ (FS)	27	Terrestrial	(*S72*, *S73*, *S75*)
West Bijou Site, Denver Basin, Colorado	2250	SQ (FS)	0.68	Terrestrial	(*S73*, *S76*)
Dogie Creek, Powder River Basin, Wyoming	2500	SP, SQ (FS)	20.8	Terrestrial	(*S73*, *S77*)
Teapot Dome, Powder River Basin, Wyoming	2500	SP, SQ (FS)	22	Terrestrial	(*S73*, *S78*)
Sussex, Powder River Basin, Wyoming	2500	SQ (FS)	26	Terrestrial	(*S73*, *S79*)
Mud Buttes, Williston Basin, SW North Dakota	2700	SP, SQ (FS)	1.36	Terrestrial	(*S73*, *S80*)
Brownie Butte, Hell Creek area, Montana	3100	SP, SQ (FS)	1.04	Terrestrial	(*S52*, *S73*, *S81*, *S82*)
Knudsen's Farm, Western Canada	3400	SQ (FS)	3.4	Terrestrial	(*S73*, *S83*)
Morgan Creek, Saskatchewan, Western Canada	3400	SQ (FS)	3	Terrestrial	(*S73*, *S84*)
Frenchman River, Saskatchewan	3400	SP	1.35	Terrestrial	(*S72*, *S85*)
Northwest Atlantic Ocean					
DSDP Leg 93 Site 603	2600	SP, SQ	n.a.	Bathyal	(*S72*, *S86*, *S87*)
ODP Leg 171 Site 1049, 1050, 1052	2400	SP, SQ	1.3	Lower bathyal	(*S88*)
ODP Leg 174AX Bass River	2500	SP, SQ, AC	n.a.	Neritic	(*S89*)
ODP Leg 207 Site 1258; 1259, 1260	4500	SP, SQ, AC	1.5	Bathyal	(*S16*, *S90*, *S91*)
Distal to Chicxulub: mm-thick K-Pg boundary event deposit					
South Atlantic Ocean					
DSDP Leg 75 Site 524	9600	n.a.	3	Abyssal	(*S92*)
ODP Leg 113 Site 690	11000	n.a.	1.5	Abyssal	(*S93*, *S94*)
ODP Leg 208 Site 1262, 1267	9400	SP, SQ	n.a.	Abyssal	(*S90*, *S95*)
Europe, Africa, Asia					
Gubbio and Petriccio, Italy	9200	SP, SQ, NI	8	Bathyal	(*S96*, *S97*)
Stevns Klint and Nye Kløv, Denmark	10200	SP, SQ, NI	48	Neritic	(*S97-S101*)
Bidart, France	9500	NI	6	Upper-middle bathyal	(*S6*, *S102-S104*)

Region and K-Pg boundary sites	Distance*	Impact ejecta**	Max. Iridium concentration	Setting***	References
	(km)		(ppb)		
Caravaca, Spain	8200	SP, SQ, NI	56	Bathyal	(*S6*, *S105*-*S107*)
Agost, Spain	8300	SP, SQ, NI	24.4	Upper-middle bathyal	(*S105*, *S108*-*S110*)
Bjala, Bulgaria	9500	SP, SQ, NI	6.1	Bathyal	(*S111*)
El Kef, Ellés, Tunisia	9100	SP, NI	18	Outer neritic – upper bathyal	(*S2*, *S6*, *S23*)
Aïn Settara, Tunisia	9100	SP, SQ, NI	11	Outer neritic – upper bathyal	(*S6*, *S112*, *S113*)
Pacific Ocean					
LL44-GPC 3	7200	SP, SQ, NI	12	Abyssal	(*S114*)
DSDP Leg 62 Site 465	7900	SP, SQ, NI	54	Lower bathyal	(*S114*-*S117*)
DSDP Leg 86 Site 576, 577	9300	SP, SQ, NI	13.4	Abyssal	(*S114*, *S118*, *S119*)
DSDP Leg 91 Site 596	9700	SP, SQ, NI	10.8	Abyssal	(*S120*)
ODP Leg 119 Site 738	10500	–	18	Abyssal	(*S121*-*S123*)
ODP Leg 130 Site 803, 807	11000	SP, SQ, NI	10.8	Abyssal	(*S114*, *S124*)
ODP Leg 145 Site 886	6450	SP, SQ, NI	3.6	Abyssal	(*S114*, *S125*)
ODP Leg 198 Site 1209 to 1212	11400	–	n.a.	Abyssal	(*S43*, *S126*)
Woodside Creek, New Zealand	10500	SP, SQ, NI (FS)	70	Bathyal	(*S14*, *S90*, *S127*, *S128*)
Mid-Waipara, New Zealand	10500	SP (FS)	0.49	Neritic	(*S129*-*S134*)
Flaxbourne River, New Zealand	10500	SP	21	Upper-middle bathyal	(*S14*, *S135*)
Moody Creek Mine, New Zealand	10500	SP (FS)	4.1	Terrestrial	(*S136*)

* Estimated paleodistance to the center of the Chicxulub crater structure.

** SP, spherules; SQ, shocked quartz; NI, Ni-rich spinel; (FS), fern spore spike.

*** We used the bathymetric division as defined in Van Morkhoven et al. (*S137*): neritic (0-200 m), upper bathyal (200-600 m), middle bathyal (600-1000 m), lower bathyal (1000-2000 m), upper abyssal (2000-3000 m), lower abyssal (>3000 m).

Table S2: Compilation of U-Pb ages from zircons from the Chicxulub impact crater, various K-Pg boundary sites, and the potential basement of the Yucatán target region (Maya Mountains, Belize).

Locality	Material	Basement age (Ma) ± 2σ*	Method	References
Chicxulub crater impactites; spherule deposit Beloc, Haiti; laminated clay layer at K-Pg boundary in Colorado	Shocked zircons	545 ± 5; 418 ± 6	U-Pb	(*S10*)
Laminated clay layer at K-Pg boundary, Colorado	Shocked zircons	550 ± 10; 571 ± 6	U-Pb	(*S138*, *S139*)
Laminated clay layer at K-Pg boundary, Saskatchewan	Shocked zircons	548 ± 8	U-Pb	(*S140*)
Silurian plutons, Maja Mountains	Zircons	418 ± 4; 404 ± 3	U-Pb	(*S141*)
Paleozoic granite	Zircons	595 ± 69; 680 ± 69	U-Pb	(*S142*)

* number refers to the last significant digits

Table S3: Quantitative mineralogy of the K-Pg boundary ejecta bed, the upper Maastrichtian ash layer, the background shales and a reference Cheto smectite from Arizona.

Mineral phases (wt%)	Cheto smectite Reference clay SAz-1	Yellow ash layer	Spherule deposit	Background shales
Quartz	1.2	5.5	1.9	17.4
Orthoclase	<0.1	0.4	0.5	1.4
Microcline	0.7	0.5	1.3	1.3
Plagioclase	9	1.6	5.7	5.5
Anorthite	0.2	0.9	0.2	0.8
Sanidine	1	3.5	<0.1	1.9
Calcite	0.6	2.2	5	7.5
Dolomite	<0.1	<0.1	0.2	0.2
Smectite	81.8	63.5	74.8	28.1
Illite1Md	4.8	13.9	5.3	28.8
Kaolinite	<0.1	1.3	2	5.4
Gypsum	0.2	4.6	0.7	0.3
Pyrite	<0.1	0.2	2.1	1.1
Goethite	<0.1	0.4	0.6	<0.1
Jarosite	0.7	1.6	<0.1	0.2

Supporting References

S1. J. Srodon, V. A. Drits, D. K. McCarty, J. C. C. Hsieh, D. D. Eberl, *Clays Clay Miner.* **49**, 514 (2001).

S2. E. Molina *et al.*, *Episodes* **29**, 263 (2006).

S3. J. J. Pospichal, *Geology* **22**, 99 (1994).

S4. S. Gardin, S. Monechi, *Bulletin de la Société Géologique de France* **169**, 709 (1998).

S5. I. Arenillas, J. A. Arz, E. Molina, C. Dupuis, *Micropaleontology* **46**, 31 (2000).

S6. E. Molina *et al.*, *Episodes* **32**, 84 (2009).

S7. W. C. Ward, G. Keller, W. Stinnesbeck, T. Adatte, *Geology* **23**, 873 (1995).

S8. B. Kettrup, A. Deutsch, *Meteor. Planet. Sci.* **38**, 1079 (2003).

S9. S. P. S. Gulick *et al.*, *Nature Geosci.* **1**, 131 (2008).

S10. T. E. Krogh, S. L. Kamo, V. L. Sharpton, L. E. Marin, A. R. Hildebrand, *Nature* **366**, 731 (1993).

S11. V. L. Sharpton, B. C. Schuraytz, K. Burke, A. V. Murali, G. Ryder, *Geol. Soc. Am. Spec. Pap.* **247**, 349 (1990).

S12. R. D. Norris, B. T. Huber, B. T. Self-Trail, *Geology* **27**, 419 (1999).

S13. B. Bauluz, D. R. Peacor, W. C. Elliott, *Earth Planet. Sci. Lett.* **182**, 127 (2000).

S14. B. Bauluz, D. R. Peacor, C. J. Hollis, *Earth Planet. Sci. Lett.* **219**, 209 (2004).

S15. M. Ortega-Huertas, F. Martínez-Ruiz, I. Palomo-Delgado, H. Chamley, *Clay Minerals* **37**, 395 (2002).

S16. P. Schulte *et al.*, Geochim. Cosmochim. Acta **73**, 1180 (2009).

S17. T. E. Yancey, R. N. Guillemette, *Geol. Soc. Am. Bull.* **120**, 1105 (2008).

S18. M. C. Harvey, S. C. Brassell, C. M. Belcher, A. Montanari, *Geology* **36**, 355 (2008).

S19. C. M. Belcher, P. Finch, M. E. Collinson, A. C. Scott, N. V. Grassineau, *Proc. Nat. Acad. Sci.* **106**, 4112 (2009).

S20. K. F. Kuiper *et al.*, *Science* **320**, 500 (2008).

S21. W. Alvarez, F. Asaro, A. Montanari, *Science* **250**, 1700 (1990).

S22. N. Robinson, G. Ravizza, R. Coccioni, B. Peucker-Ehrenbrink, R. D. Norris, *Earth Planet. Sci. Lett.* **281**, 159 (2009).

S23. G. Keller, M. Lindinger, Palaeogeogr. Palaeoclimatol. Palaeoecol. **73**, 243 (1989).

S24. R. Rocchia, E. Robin, L. Froget, J. Gayraud, *Geol. Soc. Am. Spec. Paper* **307**, 279 (1996).

S25. D. T. King,Jr., L. W. Petruny, *Geol. Soc. Am. Spec. Pap.* **437**, 179 (2007).

S26. T. F. Lawton, K. W. Shipley, J. L. Aschoff, K. A. Giles, F. J. Vega, *Geology* **33**, 81 (2005).

S27. P. Schulte, A. Kontny, *Geol. Soc. Am. Spec. Pap.* **384**, 191 (2005).

S28. A. R. Soria *et al.*, *Geology* **29**, 231 (2001).

S29. P. Schulte *et al.*, *Intern. Jour. Earth Sci.* **92**, 114 (2003).

S30. J. Smit, W. Alvarez, A. Montanari, P. Claeys, J. M. Grajales-Nishimura, *Geol. Soc. Am. Spec. Paper* **307**, 151 (1996).

S31. F. Lindenmaier *et al.*, *Chemostratigraphy of the K/T-boundary at La Sierrita and La Lajilla, NE Mexico*. (Abstracts, Geol. Soc. Am., Boulder, Colorado, 1999), pp. 123.

S32. G. Keller, W. Stinnesbeck, T. Adatte, D. Stüben, *Earth-Sci. Rev.* **62**, 327 (2003).

S33. J. A. Arz *et al.*, *J. South Am. Earth Sci.* **14**, 505 (2001).

S34. T. A. Hansen, B. Upshaw III, E. G. Kauffman, W. Gose, *Cretaceous Res.* **14**, 685 (1993).

S35. D. Heymann *et al.*, *Geochim. Cosmochim. Acta* **62**, 173 (1998).

S36. G. Keller *et al.*, *Earth Planet. Sci. Lett.* **255**, 339 (2007).

S37. J. Smit *et al.*, *Geology* **20**, 99 (1992).

S38. D. A. Kring, A. R. Hildebrand, W. V. Boynton, *Earth Planet. Sci. Lett.* **128**, 629 (1994).

S39. T. A. Hansen, R. B. Farrand, H. A. Montgomery, H. G. Billman, G. L. Blechschmidt, *Cretaceous Res.* **8**, 229 (1987).

S40. T. E. Yancey, *Gulf Coast Association of Geological Societies Transactions* **46**, 433 (1996).

S41. P. Schulte, R. P. Speijer, H. Mai, A. Kontny, *Sedim. Geol.* **184**, 77 (2006).

S42. P. Schulte *et al.*, *Earth Planet. Sci. Lett.* **269**, 613 (2008).

S43. T. J. Bralower *et al.*, *Geology* (in press) (2010).

S44. S. J. Chipera, D. L. Bish, *Clays Clay Miner.* **49**, 308 (2001).

S45. K. Goto, *Journal of the Geological Society of Japan* **111**, 193 (2005).

S46. K. Goto *et al.*, *Meteor. Planet. Sci.* **39**, 1233 (2004).

S47. J. A. Arz, L. Alegret, I. Arenillas, *Meteor. Planet. Sci.* **39**, 1099 (2004).

S48. J. Smit, S. V. D. Gaast, W. Lustenhouwer, *Meteor. Planet. Sci.* **39**, 1113 (2004).

S49. G. Keller *et al.*, *Meteor. Planet. Sci.* **39**, 1127 (2004).

S50. M. Rebolledo-Vieyra, J. Urrutia-Fucugauchi, *Meteor. Planet. Sci.* **39**, 821 (2004).

S51. S. Self, M. Widdowson, T. Thordarson, A. E. Jay, *Earth Planet. Sci. Lett.* **248**, 518 (2006).

S52. R. H. Tschudy, C. L. Pillmore, C. J. Orth, J. S. Gilmore, J. D. Knight, *Science* **225**, 1030 (1984).

S53. J. M. Grajales-Nishimura, G. Murillo-Muñetón, C. Rosales-Domínguez, E. Cedillo-Pardo, J. García-Hernández, *AAPG Mem.* **79**, 312 (2003).

S54. I. Arenillas *et al.*, *Earth Planet. Sci. Lett.* **249**, 241 (2006).

S55. T. Salge, *The ejecta blanket of the Chicxulub impact crater, Yucatán, Mexico – Petrographic and chemical studies of the K-P section of El Guayal and UNAM boreholes* (PhD, Humboldt-Universität, Berlin, Germany, 2007), pp. 190. http://edoc.hu-berlin.de/docviews/abstract.php?lang=ger&id=27753.

S56. K. O. Pope *et al.*, *Earth Planet. Sci. Lett.* **170**, 351 (1999).

S57. K. O. Pope *et al.*, *Geol. Soc. Am. Spec. Pap.* **384**, 171 (2005).

S58. B. W. Fouke *et al.*, *Sedimentology* **49**, 117 (2002).

S59. R. Tada *et al.*, *Geol. Soc. Am. Spec. Pap.* **356**, 109 (2002).

S60. S. Kiyokawa *et al.*, *Geol. Soc. Am. Spec. Pap.* **356**, 125 (2002).

S61. L. Alegret *et al.*, *Geology* **33**, 721 (2005).

S62. K. Goto *et al.*, *Cretaceous Res.* **29**, 217 (2008).

S63. G. A. Izett, *J. Geophys. Res.* **96**, 20879 (1991).

S64. H. Leroux *et al.*, *Earth Planet. Sci. Lett.* **131**, 255 (1995).

S65. B. F. Bohor, B. P. Glass, *Meteoritics* **30**, 182 (1995).

S66. L. Alegret, E. Molina, E. Thomas, *Geology* **29**, 891 (2001).

S67. J. L. Aschoff, K. A. Giles, *AAPG Bulletin* **89**, 447 (2005).

S68. C. E. Campbell, F. E. Oboh-Ikuenobe, T. L. Eifert, *Geol. Soc. Am. Spec. Pap.* **437**, 189 (2007).

S69. P. Schulte, R. Speijer, *Geologica Acta* **7**, 11 (2009).

S70. H. Sigurdsson, R. M. Leckie, G. D. Acton, *Proc. ODP Init. Rep.* **165**, 377 (1997).

S71. C. L. Pillmore, R. H. Tschudy, C. J. Orth, J. S. Gilmore, J. D. Knight, *Science* **223**, 1180 (1984).

S72. G. A. Izett, *Geol. Soc. Am. Spec. Paper* **249**, 100 (1990).

S73. D. J. Nichols, K. R. Johnson, *Plants and the K-T boundary* (Cambridge University Press, 2008), pp. 280.

S74. D. J. Nichols, C. L. Pillmore, *LPI Contribution* **38**, 3120 (2000).

S75. C. J. Orth, J. S. Gilmore, J. D. Knight, *New Mexico Geological Society Guidebook* **38**, 265 (1987).

S76. R. S. Barclay, K. R. Johnson, *Geol. Soc. Am. Field Guide* **5**, 59 (2004).

S77. B. F. Bohor, D. M. Triplehorn, D. J. Nichols, H. T. Millard,Jr., *Geology* **15**, 896 (1987).

S78. J. A. Wolfe, *Nature* **352**, 420 (1991).

S79. D. J. Nichols, J. L. Brown, M. Attrep,Jr., C. J. Orth, *Cretaceous Res.* **13**, 3 (1992).

S80. D. J. Nichols, K. R. Johnson, *Geol. Soc. Am. Spec. Paper* **361**, 95 (2002).

S81. B. F. Bohor, G. A. Izett, *Lunar Planet. Sci.* **17**, 68 (1986).

S82. A. R. Sweet, D. R. Braman, J. F. Lerbekmo, *Can. J. Earth Sci.* **36**, 743 (1999).

S83. A. R. Sweet, D. R. Braman, *Cretaceous Res.* **13**, 31 (1992).

S84. D. J. Nichols, D. M. Jarzen, C. J. Orth, P. Q. Oliver, *Science* **231**, 714 (1986).

S85. D. A. Kring, D. D. Durda, *J. Geophys. Res.* **107**, 6 (2002).

S86. G. T. Klaver, T. M. G. Van Kempen, F. R. Bianchi, *Initial Rep. Deep Sea Drill. Proj.* **93**, 1039 (1987).

S87. D. A. Kring, *J. Geophys. Res.* **100**, 16979 (1995).

S88. F. Martínez-Ruiz, M. Ortega-Huertas, I. Palomo-Delgado, J. Smit, *Geol. Soc. Am. Spec. Paper* **356**, 189 (2002).

S89. R. K. Olsson, K. G. Miller, J. V. Browning, D. Habib, P. J. Sugarmann, *Geology* **25**, 759 (1997).

S90. J. V. Morgan *et al.*, *Earth Planet. Sci. Lett.* **251**, 264 (2006).

S91. K. G. MacLeod, D. L. Whitney, B. T. Huber, C. Koeberl, *Geol. Soc. Am. Bull.* **119**, 101 (2007).

S92. K. J. Hsü *et al.*, *Science* **216**, 249 (1982).

S93. H. V. Michel, F. Asaro, W. Alvarez, L. W. Alvarez, *Sci. Res., Proc. Ocean Drill. Prog.* **113**, 159 (1990).

S94. L. D. Stott, J. P. Kennett, *Nature* **342**, 526 (1989).

S95. L. Alegret, E. Thomas, *Mar. Micropal.* **64**, 1 (2007).

S96. A. Montanari, *Jour. Sedim. Petrol.* **61**, 315 (1991).

S97. J. Smit, *Ann. Rev. Earth Planet. Sci.* **27**, 75 (1999).

S98. F. T. Kyte, Z. Zhou, J. T. Wasson, *Nature* **288**, 651 (1980).

S99. B. Schmitz, P. Andersson, J. Dahl, *Geochim. Cosmochim. Acta* **52**, 229 (1988).

S100. R. Frei, K. M. Frei, *Earth Planet. Sci. Lett.* **203**, 691 (2002).

S101. A. Trinquier, J.-L. Birck, C. J. Allègre, *Earth Planet. Sci. Lett.* **241**, 780 (2006).

S102. J. Smit, W. G. H. Z. ten Kate, *Cretaceous Res.* **3**, 307 (1982).

S103. L. Alegret, M. A. Kaminski, E. Molina, *Palaios* **19**, 574 (2004).

S104. N. Gallala, D. Zaghbib-Turki, I. Arenillas, J. A. Arz, E. Molina, *Mar. Micropal.* **72**, 196 (2009).

S105. F. Martínez-Ruiz, M. Ortega-Huertas, I. Palomo-Delgado, P. Acquafredda, *Sedim. Geol.* **113**, 137 (1997).

S106. K. Kaiho *et al.*, *Paleoceanography* **14**, 511 (1999).

S107. J. Smit, *Journal of Iberian Geology* **31**, 179 (2005).

S108. F. Martínez-Ruiz, M. Ortega-Huertas, I. Palomo-Delgado, M. Barbieri, *Chem. Geol.* **95**, 265 (1992).

S109. L. Alegret, E. Molina, E. Thomas, *Mar. Micropal.* **48**, 251 (2003).

S110. E. Molina, L. Alegret, I. Arenillas, J. A. Arz, *Journal of Iberian Geology* **31**, 137 (2004).

S111. A. Preisinger *et al.*, *Geol. Soc. Am. Spec. Pap.* **356**, 213 (2002).

S112. C. Dupuis *et al.*, *Bulletin de l'Institut Royal des Sciences Naturelles de Belgique, Sciences de la Terre* **71**, 169 (2001).

S113. D. Peryt, L. Alegret, E. Molina, *Terra Nova* **14**, 101 (2002).

S114. J. A. Bostwick, F. T. Kyte, *Geol. Soc. Am. Spec. Paper* **307**, 403 (1996).

S115. H. V. Michel, F. Asaro, W. Alvarez, L. W. Alvarez, *Initial Rep. Deep Sea Drill. Proj.* **62**, 847 (1981).

S116. P. Giblin, *Initial Rep. Deep Sea Drill. Proj.* **62**, 851 (1981).

S117. L. Alegret, E. Thomas, *Palaeogeogr. Palaeoclimatol. Palaeoecol.* **224**, 53 (2005).

S118. A. A. Wright *et al.*, *Initial Rep. Deep Sea Drill. Proj.* **86**, 799 (1985).

S119. H. V. Michel, F. Asaro, W. Alvarez, L. W. Alvarez, *Initial Rep. Deep Sea Drill. Proj.* **86**, 533 (1985).

S120. F. T. Kyte, J. A. Bostwick, L. Zhou, *Geol. Soc. Am. Spec. Pap.* **307**, 389 (1996).

S121. B. Schmitz, F. Asaro, H. V. Michel, H. R. Thierstein, B. T. Huber, *Sci. Res., Proc. Ocean Drill. Prog.* **119**, 719 (1991).

S122. B. T. Huber, *Sci. Res., Proc. Ocean Drill. Prog.* **119**, 451 (1991).

S123. A. Abrajevitch, K. Kodama, *Earth Planet. Sci. Lett.* **286**, 269 (2009).

S124. R. M. Corfield, J. E. Cartlidge, *Sci. Res., Proc. Ocean Drill. Prog.* **130**, 259 (1993).

S125. B. L. Ingram, *Sci. Res., Proc. Ocean Drill. Prog.* **145**, 399 (1995).

S126. T. J. Bralower, I. Premoli Silva, M. J. Malone, *Sci. Res., Proc. Ocean Drill. Prog.* **198**, 1 (2006).

S127. R. R. Brooks *et al.*, *Geology* **13**, 738 (1985).

S128. R. R. Brooks *et al.*, *Science* **226**, 539 (1984).

S129. R. R. Brooks *et al.*, *Geology* **14**, 727 (1986).

S130. P. S. Willumsen, *GFF* **122**, 180 (2000).

S131. P. S. Willumsen, *Journal of Micropalaeontology* **23**, 119 (2004).

S132. P. S. Willumsen, *Alcheringa* (in press) (2010).

S133. C. J. Hollis, C. P. Strong, *New Zealand Journal of Geology & Geophysics* **46**, 243 (2003).

S134. V. Vajda, J. I. Raine, *New Zealand Journal of Geology & Geophysics* **46**, 255 (2003).

S135. C. J. Hollis, C. P. Strong, K. A. Rodgers, K. M. Rogers, *New Zealand Journal of Geology & Geophysics* **46**, 177 (2003).

S136. V. Vajda, J. I. Raine, C. J. Hollis, C. P. Strong, in *Global effects of the Chicxulub impact on terrestrial vegetation: Review of the palynological record from New Zealand Cretaceous/ Tertiary boundary*, H. Dypvik, M. J. Burchell, P. Claeys, Eds. (Springer, Berlin, Germany, 2004), pp. 57-74.

S137. F. P. C. M. Van Morkhoven, B. W.A., S. A. Edwards, *Bull. Centr. Rech. Explor. - Production Elf-Aquitaine, Mémoir* **11**, 1 (1986).

S138. T. E. Krogh, S. L. Kamo, B. F. Bohor, *Earth Planet. Sci. Lett.* **119**, 425 (1993).

S139. W. R. Premo, G. A. Izett, G. P. Meeker, *Lunar Planet. Sci.* **26**, 1139 (1995).

S140. S. L. Kamo, T. E. Krogh, *Geology* **23**, 281 (1995).

S141. M. B. Steiner, J. D. Walker, *J. Geophys. Res.* **101**, 17727 (1996).

S142. R. Lopez, K. L. Cameron, N. W. Jones, *Precambrian Res.* **107**, 195 (2001).